

The Different Evolution of Gas and Dust in Disks around Sun-like and Cool Stars

I. Pascucci¹, D. Apai², K. Luhman³, Th. Henning⁴, J. Bouwman⁴, M. R. Meyer⁵, F. Lahuis⁶, A. Natta⁷

Received _____; accepted _____

¹Department of Physics and Astronomy, Johns Hopkins University, Baltimore, MD 21218

²Space Telescope Science Institute, Baltimore, MD 21218

³Department of Astronomy and Astrophysics, The Pennsylvania State University, University Park, PA 16802

⁴Max Planck Institute for Astronomy, Heidelberg, Germany

⁵Steward Observatory, The University of Arizona, Tucson, AZ 85721

⁶SRON Netherlands Institute for Space Research, Groningen, The Netherlands

⁷INAF-Osservatorio di Arcetri, 50125 Firenze, Italy

ABSTRACT

Planet formation is profoundly impacted by the properties of protoplanetary disks and their central star. However, how disk properties vary with stellar parameters remain poorly known. Here we present the first comprehensive, comparative Spitzer/IRS study of the dust and gas properties of disks around young sun-like stars (K1–M5) and cool stars/brown dwarfs (M5–M9). The comparison of these two large samples of over 60 sources reveal major differences in the evolution of both the dust and gas components.

We report the first detection of organic molecules in disks around brown dwarfs. The detection rate statistics and the line flux ratios of HCN and C₂H₂ show a striking difference between the two samples, demonstrating a significant under-abundance of HCN relative to C₂H₂ in the disk surface of cool stars. We propose this to originate from the large difference in the UV-irradiation around the two types of sources. The statistical comparison of the 10 μ m silicate emission features also reveals a difference between the two samples. Cool stars and brown dwarfs show weaker features arising from more processed silicate grains in the disk atmosphere.

These findings complement previous indications of flatter disk structures and longer disk lifetimes around cool stars. Our results highlight important differences in the chemical and physical evolution of protoplanetary disks as function of stellar mass, temperature, and radiation field which should be taken into account in planet formation models. We note that the different chemistry of pre-planetary materials in the disk may also influence the bulk composition and volatile content of the forming planets. In particular, if exogenous HCN has played a key role in the synthesis of prebiotic molecules on Earth as proposed, then prebiotic chemistry may unfold differently on planets around cool stars.

Subject headings:

1. Introduction

Circumstellar disks are a natural outcome of the star formation process and the birthplace of planetary systems. Their evolution and their lifetime determine what type of planets can form. Most studies so far have focused on characterizing protoplanetary disks around young sun-like stars (e.g. Meyer et al. 2007 for a review). It is now well established that most sun-like stars clear out their primordial dust disk in 5 Myr and only a few percent of them still retain it by an age of 10 Myr (e.g. Hernández et al. 2007). The dispersal of the gas component is less well characterized but appears to proceed equally fast (Pascucci et al. 2006; Sicilia-Aguilar et al. 2006). This rapid clearing of dust and gas around sun-like stars matches the fast growth of planetesimals and gas dispersal in the protosolar nebula as inferred from meteorites, asteroids, and planets (Pascucci & Tachibana 2009). But do disks around stars of different masses evolve similarly? Recent studies hint that disks around cool/late-type M stars, the most typical protoplanetary disks, evolve differently (e.g. Apai et al. 2008). There are at least three major differences.

First, the dispersal of primordial dust disks seems to operate less efficiently for cool stars. Carpenter et al. (2006) find that the disk frequency of low-mass stars ($\sim 0.1 - 1.2 M_{\odot}$) is statistically higher than that of higher-mass stars in the 5 Myr-old Upper Sco OB association. Infrared excess studies by Sterzik et al. (2004), Scholz et al. (2007), and Riaz & Gizis (2008) all suggest that this trend extends to the brown dwarf regime. Second, there is evidence that disks around cool stars have, on average, flatter disk structures than the more flared disks around sun-like stars (Pascucci et al. 2003; Apai et al. 2004; Allers et al. 2006 but see also the flared disks from Mohanty et al. 2004; Bouy et al. 2008). Third, the dust probed through the $10 \mu\text{m}$ silicate emission feature appears to be more processed around cool stars than around sun-like stars of similar age, suggesting more rapid grain growth in cool star disks (Apai et al. 2005; Kessler-Silacci et al. 2006).

However, there has not been a detailed comparison of the dust properties of disks around sun-like and cool stars and no investigation of their gas content. Here we present the first such comparative study. We will show that there are statistically significant differences between cool and sun-like stars in their gas and dust disk properties. First, we will demonstrate that cool stars/brown dwarfs have much weaker continuum-subtracted $10\ \mu\text{m}$ features than higher-mass stars (Sect. 3.1) implying different dust populations at the observed disk radii (Sect. 4.1). Second, we will show that HCN emission is often present in sun-like star spectra, but absent from the cool star spectra. Similarly, the median sun-like star spectrum has an HCN/C₂H₂ flux ratio that is an order of magnitude higher than the median cool star spectrum (Sect. 3.2). We will see that this arises from an under-abundance of HCN in the disk atmosphere of cool stars (Sect. 4.2). These findings highlight how stellar mass, and radiation field affect the physical and chemical evolution of protoplanetary disks including the organic compounds available during planet formation.

2. Targets, Observations, and Data Reduction

2.1. Target Selection

We compare two large samples of disks around sun-like and cool stars (including brown dwarfs) that have Spitzer spectra obtained with the same resolution and very similar signal-to-noise. The Taurus and the Cha I star-forming regions provide the best samples of protoplanetary disks to carry out our comparative study. These low-mass star forming regions are at about the same distance and do not contain early B or O type stars. In addition, their median age (~ 1 and 2 Myr) is the same within our ability to discern (see, e.g. Kenyon et al. 2008 and Luhman et al. 2008b for a review on Taurus and Cha I).

The sun-like star sample is the same as in Pascucci et al. (2008): it contains 23 single

and 21 binary stars from the Taurus-Auriga star-forming region with spectral types between K1–M5, temperatures between 3,000–5,000 K, and stellar masses between 0.4–2 M_{\odot} (see also Kenyon & Hartmann 1995 for other stellar properties). Two-thirds of the binary systems have stellar companions between 0.1''–1'', with a mean projected separation of 0.4'', or 56 AU at the distance of the Taurus star-forming region. The low-resolution IRS spectra for the sun-like star sample were acquired as part of the IRS/GTO program (Furlan et al. 2006) and have been reduced as described in Pascucci et al. (2008) and Bouwman et al. (2008). Pascucci et al. (2008) showed that there is no statistically significant difference between the strength of the 10 μm emission features from the single and binary systems in these two samples. Similarly, they showed that the ensemble of spectral energy distributions is indistinguishable between the single and binary system samples.

Our cool star sample includes objects with spectral types between M5–M9, stellar temperatures between \sim 2,500–3,000 K and masses between \sim 0.04–0.15 M_{\odot} (see Table 1 and also Apai et al. 2005; Luhman 2007). These objects were selected from the Cha I star-forming region following two main criteria: i) reliable spectral classification, and ii) mid-infrared excess emission. We used the optical/infrared surveys by Comerón et al. (2000), López-Martí et al. (2004), Luhman (2004), and Luhman et al. (2005) to identify sources close to or below the substellar boundary. We then correlated these sources with the ISO/ISOCAM detections at 6.7 and 14.3 μm from Persi et al. (2000) and the Spitzer/IRAC 8 μm fluxes from Luhman et al. (2008a). The ISOCAM–selected sample consists of eight sources: Hn 2, CHXR 15, Cha H α 1, Cha H α 9, Cha H α 2, ISO 138, Cha H α 6, and ISO 217. These sources were observed in March 2005 as part of our Cycle–1 Spitzer proposal and were selected to have fluxes larger than 10 mJy in at least one of the two wavelengths to ensure a reliable detection of excess emission. Another eleven sources were selected later based on excess emission in the IRAC 5.8 and/or 8 μm bandpasses (Luhman et al. 2008a), and were observed as part of our Cycle–3 Spitzer proposal in August 2006 and March 2007.

The IRAC–selected sources are: ESO H α 559, ISO 79, CHSM 9484, Cha 23943, ISO 147, Cha 9086, T37, ISO 165, ISO 252, Hn 13, and Cha 21330.

2.2. Cool Star Sample: Observations

We used the infrared spectrograph (IRS, Houck et al. 2004) on–board the Spitzer Space Telescope to perform low–resolution ($R \sim 64\text{--}128$) spectroscopy of the $10\ \mu\text{m}$ silicate emission feature of the selected cool stars. We employed for all sources the SL1 module covering the wavelength range between $7.4\text{--}14.5\ \mu\text{m}$. For several sources of the Cycle–1 proposal we also adopted the LL1 module ($19.5\text{--}38.0\ \mu\text{m}$) aiming to probe solid–state features at long wavelengths. However, because most of the selected brown dwarfs turned out to have flat disk structures (Apai et al. 2005), the signal–to–noise ratio of the LL1 observations is only modest. This means that we can use the LL1 data only to trace the infrared continuum. In view of this finding, we preferred to drop the LL1 module for the Cycle–3 observations. We chose instead the SL2 module ($5.2\text{--}7.7\ \mu\text{m}$) to better establish the continuum slope around the $10\ \mu\text{m}$ silicate emission feature. The parameters of the observations are summarized in Table 2. Most of the sources were centered in the spectrograph slit using the high–accuracy PCRS mode ($1\ \sigma$ positional uncertainty of $0.4''$). The exceptions are Cha 9086, ISO 217, and Hn 13 where no suitable optical reference star was available. For these sources, we used the medium accuracy infrared peak–up array integrated onto the IRS focal plate providing a $1\ \sigma$ positional uncertainty of $1''$. All peak–up operations were successful and no significant flux loss is expected from any of our sources. Each source was checked individually to confirm that only one point source was covered by the slit. We used fixed cluster offset–mode observations and grouped nearby targets to reduce the telescope overhead. By using the staring mode observation template, we acquired each target in two nod positions along the spatial direction of the slit, at $1/3$ and

2/3 of the slit length.

2.3. Data Reduction

The sun-like and cool star samples have been reduced in an identical way, with only very minor differences. We have already published the spectra of the sun-like star sample in Pascucci et al. (2008). Here we adopted the already reduced spectra from our previous paper and will now only discuss the reduction of the cool star sample.

The cool star data have been processed through the SSC pipeline version S15.3.0 and S16.1.0. Our goals required a data quality higher than that produced by the SSC pipeline. We start our data reduction from the so-called *droopres* products and use the SMART reduction package (Higdon et al. 2004), in combination with IDL routines developed for the FEPS Spitzer Science Legacy program (Meyer et al. 2006). The data reduction steps are outlined in detail in Bouwman et al. (2008) and have been successfully used in a series of publications (see, e.g. Meyer et al. 2004; Apai et al. 2005; Bouwman et al. 2006; Pascucci et al. 2008). In brief, we first subtracted the pairs of imaged spectra acquired along the spatial direction of the slit to correct for background emission, stray light, and pixels with anomalous dark current. We replaced pixels flagged as bad by the SSC pipeline (and additional 3-4 pixels per frame identified by eye) by interpolating over neighboring good pixels. Spectra were extracted from the background-subtracted pixel-corrected images using a 6-pixel fixed-width aperture in the spatial direction.

Because all targets have been acquired with a high or moderate peak-up option (pointing accuracy within 0.4-1") and the majority are too faint to perform source profile fitting, we opted to fix the position of the aperture for each spectral order to that derived by the FEPS legacy program. After extracting the spectra for each order, nod, and cycle, we

computed a mean spectrum for each order and as uncertainty we quoted the 1σ standard deviation of the distribution of the flux densities measured at the given wavelength. We converted our output spectra to flux by applying the spectral response function derived by the FEPS Legacy team (Bouwman et al. 2008), and propagate the calibration error into the quoted uncertainties.

3. Results

The SL1 observations detected all cool stars and achieved a sub-mJy accuracy. We confirm the ISOCAM excess emission detections in all but two sources: Our Spitzer/IRS observations of Hn 2 and CHXR 15 show flux densities fully consistent with photospheric emission and we identify no hints of the ISOCAM excess emission reported by López-Martí et al. (2004). It seems likely that these two sources have been missclassified: photospheric emission from sources earlier than our spectral type limit of M6 can fully explain the ISOCAM observations (Luhman et al. 2008a, see also Table 1). We excluded these two sources from the following analysis and discussion. In addition, we find that ISO 138 has IRS excess emission inconsistent with the ISOCAM photometry (Persi et al. 2000; López-Martí et al. 2004), but fully consistent with the IRAC $8\mu\text{m}$ by Luhman et al. (2008a), see also Fig. 2. The IRS and the IRAC fluxes at $8\mu\text{m}$ are about eight times lower than the ISOCAM flux at $6.7\mu\text{m}$. We suspect that the source 2MASS 11082238-7730277 at $\sim 18''$ from ISO 138 has contaminated the ISOCAM estimates by López-Martí et al. (2004).

The LL1 observations detected all disks in our sample. The low LL1 fluxes confirm the previous suspicion that most very low mass objects have flatter disk structures (Apai et al. 2005). However, given the low S/N these observations do not further our understanding of the dust composition and will not be discussed in the rest of the paper.

We find that 14 out of 17 cool star disks have $10\ \mu\text{m}$ silicate emission features. These, combined with the sun-like stars and the Herbig Ae/Be stars as described in Sect. 3.1, make a sample of 72 disks where the dust properties can be studied as a function of stellar mass/luminosity. To compute the strength of the $10\ \mu\text{m}$ features we followed the procedure described in Pascucci et al. (2008). The continuum below the feature is estimated as follows. For the sources that have IRS spectra covering the wavelength region between $5.3\text{--}14.2\ \mu\text{m}$ we fit a third-order polynomial between 6 and $8\ \mu\text{m}$ and between 12 and $14\ \mu\text{m}$. These sources comprise all the sun-like stars and the following cool stars: ESO-H α 559, ISO 79, CHSM 9484, ISO 147, T37, ISO 165, ISO 252, and Hn 13. For sources that have a smaller wavelength coverage we fit a first order polynomial between the minimum wavelength and $8.2\ \mu\text{m}$ and between $12\ \mu\text{m}$ and the maximum wavelength. The sources belonging to the last sample are all the Herbig Ae/Be disks and the following cool stars: Cha H α 1, Cha H α 9, Cha H α 2, ISO 138, Cha H α 6, and ISO 217.

We report the detection of the ν_5 vibration-rotation band of acetylene (C_2H_2) around $13.7\ \mu\text{m}$ and of the ν_2 band of hydrogen cyanide (HCN) around $14.0\ \mu\text{m}$ toward at least 20 disks in the combined sample of sun-like and cool stars (Sect. 3.2). We identify the ν_5 and ν_2 bands of C_2H_2 and HCN using the following procedure. First, we fit a linear continuum in a wavelength region outside the expected emission bands (between $13.4\text{--}13.60\ \mu\text{m}$ and $14.15\text{--}14.3\ \mu\text{m}$). Then, we integrate the flux of the continuum-subtracted spectra within the wavelength region of the low-resolution spectrum where the emission bands are expected to be ($13.6\text{--}13.81\ \mu\text{m}$ for C_2H_2 and $13.81\text{--}14.15\ \mu\text{m}$ for HCN). The uncertainty on the measured band flux is dominated by two errors: a) the error on the continuum subtraction, which we compute as the standard deviation of the pixels outside the emission feature in the continuum-subtracted spectrum; and, b) the propagation of the measurement errors at each pixel. We classify emission bands as “firm” detections or “possible” detections, based on the S/N values derived above. We successfully confirmed this classification by individually

inspecting every spectra by eye. In the case of the cool star sample possible detections have S/N between 2 and 5 while all firm detections have a $S/N > 7$. In the case of the sun-like sample the S/N estimate is more uncertain for two reasons: i) the fit of the continuum is less certain because the continuum is less flat than that from cool star spectra; ii) the errors at each wavelength are more uncertain because the sun-like stars have only 4 exposures per nod position (for comparison cool stars have more than 10 exposures per nod). Most firm identifications have S/N greater than 3 in the sun-like star sample (possible identifications have S/N slightly lower than 3). Five out of 17 cool star disks have “firm” detections of C_2H_2 , other 4 sources have possible detections. Only 1 cool star shows a “possible” detection of the HCN rovibrational emission band. Among the 44 sun-like stars, there are 4 “firm” and 3 more “possible” detections of C_2H_2 , while there are 13 “firm” detections and 7 more “possible” detections of HCN (see also Table 3).

3.1. Weak Silicate Emission Features in Cool Star Disks

Grains from the interstellar medium (ISM) provide the initial solids that comprise forming circumstellar disks. These grains are likely a mixture of silicates and carbon with a range in size from a few tens of Å up to $\sim 0.2 \mu\text{m}$ (see, e.g. Draine 2003; Gail & Hoppe 2009). The $10 \mu\text{m}$ absorption features toward several lines of sight show that most of the silicates are amorphous and crystalline material constitutes less than 2% by mass (Kemper et al. 2005). These primordial grains undergo major chemical and physical changes during and after the formation of circumstellar disks, some of which are reflected in the $10 \mu\text{m}$ silicate emission feature. Silicate emission features from our targets show a considerable diversity ranging from the strong, sharp feature of Cha H α 1 to the almost featureless spectra of J11082570, J11084952, and J11112249.

The qualitative spectral comparison in Fig. 5 shows that dust in the disks of cool stars

is more processed than it is in the ISM (see also Apai et al. 2005). In fact, these disks have a broad, flat-topped $10\ \mu\text{m}$ emission band, indicative of grains larger than the $0.1\ \mu\text{m}$ grains that dominate the ISM. In addition, most spectra show peaks at 9.4 and $11.3\ \mu\text{m}$ from crystalline silicates similar to those identified in spectra of comets (e.g., Wooden et al. 2007).

Van Boekel et al. (2003) first identified a correlation between the shape and the strength of the $10\ \mu\text{m}$ silicate emission features from disks around intermediate-mass stars (Herbig Ae/Be stars). This correlation was interpreted in terms of dust evolution and is often used to characterize the amount of “primitive” versus “processed” dust in disk atmospheres. We have re-analyzed the Herbig Ae/Be sample from van Boekel et al. (2005) and expanded the analysis to disks around young sun-like stars (from the sample studied in Pascucci et al. 2008) and cool stars (from this work). In Fig. 6, we show the flux ratio of the continuum-subtracted spectra at 11.3 and $9.8\ \mu\text{m}$ versus the peak-over-continuum flux density within the $10\ \mu\text{m}$ emission feature. Features dominated by “primitive” dust (sub-micron amorphous grains like those in the ISM) have low $11.3/9.8$ ratios and high peak-over-continuum fluxes. In contrast, features dominated by “processed” dust (micron-sized grains and crystals) are characterized by high $11.3/9.8$ ratios and low peak-over-continuum fluxes. This figure confirms the trend we reported in Apai et al. (2005): disks of cool stars have silicate emission features dominated by “processed” dust, the extent of processing is typically higher than in disks around sun-like and Herbig Ae/Be stars. Recently, Kessler-Silacci et al. (2006) compared the strength of the silicate emission feature from disks around 13 Herbig Ae/Be stars to that from disks around 15 M stars and found a probability as large as $\sim 15\%$ that these two groups are drawn from the same parent population. We applied the Kolmogorov-Smirnov (K-S) test to our much larger sample of Herbig Ae/Be, sun-like and cool stars. We find that the feature strengths from the Herbig Ae/Be and sun-like star disks and from the sun-like star and cool star disks

are also consistent with being drawn from the same parent population (K-S probabilities of 6 and 7% respectively). On the other hand, the samples of cool star and Herbig Ae/Be disks statistically differ in the *strength* of their $10\ \mu\text{m}$ emission features (K-S probability of 0.6%), with cool star disks having weaker features than Herbig Ae/Be disks. The *shape* of the $10\ \mu\text{m}$ emission feature is not statistically different among the three samples of disks (P(cool:sun-like)=7%, P(cool:Herbig)=16%, P(sun-like:Herbig)=6%). Note that the mean value of the peak-over-continuum becomes larger going from the disks of cool stars, through the sun-like stars, to the Herbig Ae/Be stars (see Fig. 6). In Sect. 4.1 we will discuss a scenario that can explain the observed trend between the strength of the silicate features and the stellar mass/luminosity.

3.2. Low HCN/C₂H₂ Flux Ratios in Cool Star Disks

The most exciting result of our survey has been the discovery of the vibration-rotation bands of C₂H₂ and HCN in at least 5 out of 17 cool stars with disks (Figs. 1, 2, 3, 4). No organic molecules have been previously detected toward such very low-mass stars. Motivated by the high detection rate, we have searched for the presence of the C₂H₂ and HCN bands in the sun-like star sample. We find that at least 15 out of 44 sun-like spectra exhibit emission from C₂H₂ and/or HCN (Figs. 7, 8, 9, 10). The sample of sun-like stars consists of about an equal number of single and binary stars (Pascucci et al. 2008). The detection rate of C₂H₂ and HCN among single stars is similar to that among binary stars. Therefore, in the following we will not distinguish between single and binary stars, but rather contrast the sun-like star sample to the cool star sample.

First, we note that the overall detection rate of C₂H₂ and HCN is very similar in the sun-like star and cool star samples, with $\sim 30\%$ of the disks showing emission bands in the Spitzer low-resolution spectra. We searched for any correlation between the presence of gas

lines and the dust disk properties, such as the strength of the $10\ \mu\text{m}$ emission feature and the infrared slope of the source spectral energy distribution¹. Since the 44 sun-like stars were selected to have silicate emission features from optically thin disk atmospheres, we excluded the 3 featureless cool stars from this comparison (J11082570-7716396, J11084952-7638443, J11112249-7745427). Fig. 11 shows the histograms of the peak-over-continuum ratios of the $10\ \mu\text{m}$ silicate emission features for the detections and for the non-detections of the C_2H_2 and HCN rovibrational bands. Detections are only present in disks with weak silicate emission features (peak-over-continuum ratios < 2). In addition, detections are confined to those disks with evidence for flatter geometries (Fig. 12). In summary, the disks with gas detections show clear signs of grain growth and dust settling both among the sun-like and the cool star samples. This correlation may be an observational bias. Disks with larger grains and flatter disk geometries have weaker mid-infrared continuum levels making it easier to detect gas emission lines (see, e.g. Pascucci et al. 2007).

When inspecting the detection rates of C_2H_2 and HCN separately, we find a striking difference between the samples of sun-like and cool stars. C_2H_2 is detected in at least 5 out of 14 cool star spectra with silicate emission features, but at most in 7 out of 44 sun-like stars (only 4 are considered 'firm' detections). In contrast, only the single cool star spectrum of Cha H α 2 presents a possible HCN emission band, but at least 13 sun-like stars have HCN detected (see Table 3). In addition, the band strengths of C_2H_2 and HCN are different in the two samples. Emission from HCN is brighter than that from C_2H_2 in most disks around sun-like stars (a notable exception is CY Tau). In contrast, all disks around cool stars have brighter C_2H_2 emission compared to HCN. This trend is well illustrated in Fig. 14, where we plot the median (at each wavelength) of the continuum-subtracted and

¹for this we used the IRS fluxes at 7 and $13\ \mu\text{m}$, and the MIPS $24\ \mu\text{m}$ data from Pascucci et al. (2008) and Luhman et al. (2008a)

normalized spectra for the sun-like and the cool stars with C₂H₂ and/or HCN emission band detections. The flux ratio of HCN over C₂H₂ is ~ 2.9 for the median sun-like star spectrum, while it is only 0.26 for the median cool star spectrum. The only two sources where both C₂H₂ and HCN are firmly detected are the sun-like stars DF Tau and CoKu Tau 3 with HCN over C₂H₂ flux ratios of ~ 1.3 and 0.7, respectively (see Fig. 14). These two objects alone point to a diversity in the line flux ratios of HCN and C₂H₂ in sun-like stars. This diversity should be further investigated with sensitive high-resolution Spitzer spectra. We stress, that the differences in detection frequency and band strength between the sun-like and cool stars are not explained by possible differences in the infrared continuum, its shape, and signal-to-noise ratio among the two samples because the C₂H₂ and HCN bands are at adjacent wavelengths. Sect. 4.2 suggests a possible scenario to explain these findings.

4. Discussion

4.1. Dust Processing, Stellar Luminosity and Disk Turbulence

The main result of Sect. 3.1 is the trend between the stellar mass/luminosity and the strength of the 10 μm silicate emission feature with disks around Herbig Ae/Be stars having statistically stronger features than disks around cooler/lower-mass stars. In other words, the 10 μm emission features from disks around low-mass/luminosity stars are dominated by more “processed” dust than the same features from disks around higher mass/luminosity stars. How can we explain this observational trend?

The 10 μm silicate emission feature arises from different regions in disks around stars of different luminosities. Kessler-Silacci et al. (2007) calculated that it probes radii $\geq 0.5\text{--}50$ AU in disks around Herbig Ae/Be stars, but only radii $\leq 0.001\text{--}0.1$ AU in brown dwarf disks. This fact may provide an explanation to our observations. The closer the

grains are to the central star the faster they are depleted due to the higher density and rotational frequency which enhance the collision rate of dust grains and the velocity at which particles settle to the disk midplane. In this picture, the grain sizes inferred from the $10\ \mu\text{m}$ silicate features are not representative for the bulk silicate dust in the disk but rather reflect the different location of the $10\ \mu\text{m}$ emission zone around stars of different luminosities (see also Apai et al. 2005; Kessler-Silacci et al. 2007). However, grain growth and dust settling are not the only mechanisms determining the grain size distribution in the disk atmosphere.

Turbulence may also affect the strength of the $10\ \mu\text{m}$ emission feature, for instance by stirring up large grains from the disk midplane. In the frame of the magnetorotational instability model (Balbus & Hawley 1991), stellar accretion rates are a good proxy for the disk turbulence (Gammie 1996). In Fig. 13 we plot the strength of the $10\ \mu\text{m}$ emission features versus the stellar accretion rates for the sample of sun-like stars. The upper envelope of this plot suggests a trend with high accretion rate systems having large grains and moderate/low-accretion rate systems having small grains. However, the large uncertainty in the stellar accretion rates precludes any firm conclusion. This, in addition to the fact that large grains are seen commonly at all accretion rates, suggests that accretion/turbulence can only play a minor role in determining the strength of the $10\ \mu\text{m}$ silicate emission feature.

Finally, it should be also noted that disk models including only dust coagulation and settling/vertical mixing produce a too rapid (only 10^4 years) depletion of grains up to $100\ \mu\text{m}$ in size essentially at all disk radii (Dullemond & Dominik 2005), which is inconsistent with the frequent detection of $10\ \mu\text{m}$ emission features in Myr-old disks. Fragmentation of aggregate grains could be the major mechanism replenishing the population of small grains. Brauer et al. (2008) implemented aggregate fragmentation in their disk model and

show that grain growth and fragmentation can reach an equilibrium for a period of $\sim 10^6$ which results in a quasi-stationary grain size distribution. If the average grain size of quasi-stationary grain size distributions decreases with radial distance from the central star then such disk models could explain our observations.

4.2. HCN under-abundance in Disk Atmospheres of Cool Stars

We have shown in Sect. 3.2 that there is a striking difference in the detection rates of HCN and C₂H₂ between the sun-like and the cool star samples. HCN is often present in sun-like star spectra, but absent from the spectra of cool stars. Similarly, Fig. 14 demonstrates that the HCN/C₂H₂ flux ratio is much higher toward sun-like stars than toward cool stars. As explained below, these differences arise from different abundances in the two samples.

To model the emission from the ν_5 band of C₂H₂ and the ν_2 band of HCN we followed the procedure described in Lahuis & van Dishoeck (2000), which assumes rotational and vibrational levels in local thermal equilibrium. Using the populations in each level, the optical depths are calculated assuming a Voigt profile function. The spectrum is also multiplied at each frequency by the black body emission of gas at the temperature T_{gas} and reduced to the resolution of the IRS/SL module using a Gaussian profile. First, we explored whether our low-resolution spectra can provide any interesting constraints on T_{gas} . To do that, we have simulated spectra with gas temperatures from 100 to 900 K and measured the shift in the band head peak emission. The peak emission of the ν_2 band of HCN shifts from 14.02 μm for $T_{\text{gas}}=100$ K to 13.96 μm for $T_{\text{gas}}=900$ K. This shift is about half the spectral resolution of the IRS/SL1 module at 14 μm and cannot be reliably detected in our spectra. A similar result is reached for the ν_5 band of C₂H₂. We find that the wavelengths at which the emission of HCN and C₂H₂ peak in the observed spectra are in between the predicted

peaks for gas at 100 K and 900 K. In summary, the resolution of our spectra is not sufficient to measure the temperature of the emitting gas, but it is fully consistent with the emitting gas having temperature between 100 K and 900 K.

More excitingly, the HCN/C₂H₂ flux ratio informs us on the relative column densities of the two molecules. We computed synthetic spectra with varying column density ratios of HCN over C₂H₂, calculated the line flux ratios and compared them to the observed line flux ratios in the sun-like and cool star samples (see Fig. 15). Absorption spectra of HCN and C₂H₂ toward young embedded massive stars find highly correlated excitation temperatures for these molecules demonstrating that they probe warm gas at similar temperatures (Lahuis & van Dishoeck 2000). We consider here three temperatures for the HCN and C₂H₂ emitting gas: 650 K, which Carr & Najita (2008) find to fit best the HCN and C₂H₂ band profiles from AA Tau, 450 and 850 K as comparison temperatures. Other important model parameters are the gas column densities and Doppler broaden line widths. In our calculations we keep the C₂H₂ column density fixed to 10^{16} cm^{-2} while we vary the HCN column density between $0.5\text{-}11^{16} \text{ cm}^{-2}$, thus covering the column densities derived by Carr & Najita (2008) for AA Tau. We also assume a Doppler line broadening of 5 km/s, greater than the thermal broadening for the considered temperature range. The strongest C₂H₂ and HCN emission lines start to become optically thick around 10^{16} cm^{-2} and $7 \times 10^{16} \text{ cm}^{-2}$, respectively, for gas temperatures $\geq 400 \text{ K}$ (see Fig. 3 from Lahuis & van Dishoeck 2000). Fig. 15 shows that, regardless of the gas temperature, HCN/C₂H₂ line flux ratios as high as 3 can be obtained only for large HCN/C₂H₂ column density ratios. The line ratio is almost independent from the gas temperature because both the C₂H₂ and the HCN lines start to become only marginally thick for the parameters we considered. If we assumed higher column densities for the two molecules or smaller Doppler line broadening, the HCN over C₂H₂ line flux ratio would start to saturate faster and even higher HCN/C₂H₂ column density ratios would be required to obtain the typical

HCN/C₂H₂ line ratio of 3 of sun-like stars. In contrast, the low HCN/C₂H₂ flux ratio measured in cool stars must originate from a lower column density of HCN in respect to C₂H₂. For comparison, Lahuis & van Dishoeck (2000) and Boonman et al. (2003) find that HCN is a factor of a few more abundant than C₂H₂ in hot molecular cores. How can we explain the HCN under-abundance in the disk atmospheres of cool stars?

Here we propose a possible explanation. If HCN is formed in the warm disk atmosphere then its abundance may be limited by the availability of gas-phase atomic N (e.g. Agundez et al. 2008). Atomic N is primarily produced via the photo-dissociation of N₂, thought to be the most abundant nitrogen-bearing molecule in the interstellar medium (Bergin et al. 1995). Thus, the HCN abundance may be limited by Φ_{uv} , the flux of UV-photons with $\lambda < 110$ nm, required to dissociate N₂². For young stars Φ_{uv} is dominated by emission of hot ($\sim 10,000$ K) gas accreting onto the stars (Matsuyama et al. 2003; Herczeg et al. 2004). A simple estimate for the accretion luminosities of the two samples suggests that their Φ_{uv} differ by more than 3 orders of magnitude, although the stellar temperatures differ by only 30% (Table 3). If the HCN production from N is indeed driven by the UV-photochemistry, the large difference in the UV flux of sun-like and cool stars may naturally explain our observations. An important consequence of this scenario is the general under-abundance of molecular species produced through UV chemistry and an over-abundance of molecules with large binding energies in cool star disks. With efficient vertical and radial mixing (e.g., Ciesla 2007), the composition of the disk atmosphere may be representative of the overall disk composition. Indeed, turbulent mixing seems to be necessary to explain the high abundances of warm HCN and C₂H₂ in the only single disk

²While the dissociation of NH₃ could also provide free N, van Dishoeck et al. (2008) show that photodissociation rates for this molecule are insensitive to the radiation field for temperatures between 10,000 and 4,000 K

atmosphere where they were detected previously (Carr & Najita 2008). Detailed dust and gas disk modeling is required to understand whether the UV-photochemistry in the disk atmosphere can radically affect the organics in the disk midplane.

An alternative, though perhaps less likely explanation is that our observations are tracing cometary or interstellar ice evaporation, in which case the organics in the disk midplane may not be different. DiSanti & Mumma (2008) have shown that Oort cloud comets have an HCN/C₂H₂ ratio near unity, but Jupiter family comets have less C₂H₂. Because the HCN abundance relative to water is high by interstellar standards in Oort cloud comets, HCN seem to form efficiently in the outer disk, perhaps via surface chemical reactions on icy dust grains (Charnley et al. 1992). Nonetheless, the evaporation of cometary ices alone cannot reproduce our results, unless C₂H₂ is preferentially destroyed in the disk atmospheres of sun-like stars. C₂H₂ has a dissociation cross-section that is at least an order of magnitude higher than HCN for photons with λ between 1300–2000 Å (Lee 1984). Because sun-like stars have more flux than cool stars at these wavelengths, C₂H₂ could be more easily destroyed in the disk atmosphere of sun-like stars. However, it is interesting to consider how photodissociation rates depend on the stellar radiation field (Table 2 from van Dishoeck et al. 2008). Going from a stellar radiation field produced by a star of 10,000 K to that of a 4,000 K star the C₂H₂ photodissociation rate decreases only by a factor of 9, that of HCN by a factor of 68, while that of N₂ by more than 4 orders of magnitudes. Based on this dependence on the temperature of the radiation field, it seems more likely that the large difference in HCN/C₂H₂ abundance is caused by more efficient dissociation of N₂ in disk atmospheres of accreting sun-like stars.

4.3. On the Organics Available During Planet Formation

HCN is the key building block of many complex organic compounds. Under reducing conditions the polymerization of five HCN molecules can form adenine (Oro 1960), one of the two purine nucleobases at the core of the replication system of all terrestrial organisms. But even if the early Earth atmosphere was reducing, the synthesis of adenine through HCN polymerization under terrestrial conditions remains controversial (Shapiro 1995) and its delivery through cometary or meteoritic impacts has been proposed as a likely alternative (Chyba & Sagan 1992). Adenine synthesis likely occurs in extraterrestrial environments (Stoks & Schwartz 1981; Kissel & Krueger 1987), consistent with the observations of abundant HCN in the interstellar space (Hirota et al. 1998), in comets (Magee-Sauer et al. 2002) and recently in disks (this work, Lahuis et al. 2006; Gibb et al. 2007; Najita et al. 2007). In addition, the availability of simple organic molecules such as HCN has a fundamental impact on the chemical networks in protoplanetary disks (Semenov et al. 2004) and thus on the compounds available during planet formation.

Our observations show that HCN is under-abundant in the disk atmosphere of cool stars. With efficient mixing in the disk, this finding may reflect an overall deficiency of HCN in disks around cool stars. In this case, it is possible that the organics in the planet forming regions of cool stars, as well as the organics possibly delivered post-formation, will differ from those around sun-like stars. If exogenous HCN has played a key role in the synthesis of prebiotic molecules on Earth as proposed, then prebiotic chemistry may unfold differently on planets around cool stars.

5. Summary

Using Spitzer/IRS we compared the gas and dust properties of 17 disks around cool stars/brown dwarfs to 58 disks around sun-like and intermediate-mass stars. The cool stars have spectral types later than M5, the sun-like stars between K1 and M5, and the intermediate-mass stars have spectral types earlier than A0. As the first large comparison, we found important and surprising differences between these samples. Our results can be summarized as follows:

1. We identify 14 cool star disks with $10\ \mu\text{m}$ silicate emission features. Features are broad and weak suggesting that grains at least a few-microns in size are present in the disk atmospheres. Most of the cool star spectra also show prominent crystalline silicate features.
2. The sample of disks around cool and intermediate-mass stars statistically differ in the strength of their $10\ \mu\text{m}$ emission features, with cool stars having much weaker continuum-subtracted features than intermediate-mass stars. The observed difference demonstrates that the dust populations at the observed disk radii are different in the two samples.
3. We report the first detections of organic molecules from disks around brown dwarfs.
4. We find a striking difference in the detection rates of HCN and C_2H_2 between the sun-like and the cool star samples, with HCN often present in sun-like stars, but absent from the cool star spectra. Similarly, the HCN/ C_2H_2 flux ratio of the median sun-like star spectrum is an order of magnitude higher than that of the median cool star spectrum. We interpret these as evidence for different abundances of the two molecules in the disk atmosphere of sun-like and cool stars. Efficient photodissociation of N_2 in the disk atmosphere of sun-like stars may drive the higher production of

HCN.

We would like to thank S. Strom, J. Najita, and J. Carr for interesting discussions. I. P. thanks T. Heran who contributed to the realization of Fig. 13 in the frame of the NASA Space Grant Program. K. L. was supported by grant AST-0544588 from the National Science Foundation. This work is based on observations made with the Spitzer Space Telescope, which is operated by the Jet Propulsion Laboratory, California Institute of Technology. We are pleased to acknowledge support through the NASA/RSA contract number 1351891. M. R. M. acknowledges the support of the NASA Astrobiology Institute through LAPLACE.

Facilities: Spitzer Space Telescope

REFERENCES

- Allers, K. N., Kessler-Silacci, J. E., Cieza, L. A., Jaffe, D. T. 2006, *ApJ*, 644, 364
- Apai, D., Pascucci, I., Sterzik, M. F., van der Blik, N., Bouwman, J., Dullemond, C. P., Henning, Th. 2004, *A&A*, L426, 53
- Apai, D., Pascucci, I., Bouwman, J., Natta, A., Henning, Th., Dullemond, C. P. 2005, *Science*, 310, 834
- Apai, D., Luhman, K., Liu, M. C. 2008, 14th Cambridge Workshop on Cool Stars, Stellar Systems, and the Sun ASP Conference Series, Vol. 384,
- Agundez, M., Cernicharo, J., Goicoechea, J. R. 2008, *A&A* in press
- Balbus, S. A. & Hawley, J. F. 1991, *ApJ*, 376, 214
- Bergin, E. A., Langer, W. D., Goldsmith, P. F. 1995, *ApJ*, 441, 222
- Boonman, A. M. S., van Dishoeck, E. F., Lahuis, F., Doty, S. D., Wright, C. M., Rosenthal, D. 2003, *A&A*, 399, 1047
- Bouy, H., Huélamo, N., Pinte, C. et al. 2008, *A&A*, 486, 877
- Bouwman, J. et al. 2006, *ApJ*, L653, 57
- Bouwman, J. et al. 2008, *ApJ*, 683, 479
- Brauer, F., Dullemond, C. P., Henning, Th. 2008, *A&A*, 480, 859
- Carpenter J. M., Mamajek, Eric E., Hillenbrand, L. A., Meyer, M. R. 2006, *ApJ*, L651, 49
- Carr, J. S. & Najita, J. R. 2008, *Science*, 319, 1504
- Charnley, S. B., Tielens, A. G. G. M., Millar, T. J. 1992, *ApJ*399, L71

- Chyba, C. F. & Sagan, C., *Nature* 1992, 355, 125
- Ciesla, F. J. 2007, *Science* 318, 613
- Comerón, F., Neuhauser, R., Kaas, A. A 2000, *A&A*, 359, 269
- Crovisier, J., Leech, K., Bockelee-Morvan, D., Brooke, T. Y., Hanner, M. S., Altieri, B., Keller, H. U., Lellouch, E. 1997, *Science*, 275, 1904
- Cutri, R. M. et al. 2003, 2MASS All Sky Catalog of point sources
- D'Alessio, P., Calvet, N., Hartmann, L., Lizano, S., Cant, J. 1999, *ApJ*, 527, 893
- Disanti, M. A. & Mumma, M. J. 2008, *Space Science Reviews*, 70
- Draine, B. T. 2003, *ARA&A*, 41, 241
- Dullemond & Dominik 2005, *A&A*, 434, 971
- Furlan, E., Hartmann, L., Calvet, N. et al. 2006, *ApJS*, 165, 568
- Gail, H. & Hoppe, P. 2009, to appear in the book *Protoplanetary Dust*, eds. D. Apai & D. Loretta (Cambridge University Press)
- Gammie, C. F. 1996, *ApJ*, 462, 725
- Gibb, E. L., Van Brunt, K. A., Brittain, S. D., Rettig, T. W. 2007, *ApJ*, 660, 1572
- Gullbring, E., Hartmann, L., Briceno, C., Calvet, N. 1998, *ApJ*, 492, 323
- Hartigan, P., Edwards, S., Ghandour, L. 1995, *ApJ*, 452, 736
- Hartmann, L., Calvet, N., Gullbring, E., D'Alessio, P. 1998, *ApJ*, 495, 385
- Hartmann, L. 2001, *AJ*, 121, 1030

- Herczeg, G. J., Wood, B. E., Linsky, J. L., Valenti, J. A., Johns-Krull, C. M., *Astrophys. J.* 2004, 607, 369
- Hernández, J., Hartmann, L., Megeath, T. et al. 2007, *ApJ*, 662, 1067
- Higdon, S. J. U., Devost, D., Higdon, J. L. et al. 2004, *PASP*, 116, 975
- Hirota, T., Yamamoto, S., Mikami, H., Ohishi, M. 1998, *ApJ*, 503, 717
- Houck, J. R., Charmandaris, V., Brandl, B. R. et al. 2004, *ApJS*, 154, 211
- Kemper, F., Vriend, W. J., Tielens, A. G. G. M. 2005, *ApJ*, 633, 534
- Kenyon, S. J. & Hartmann, L. 1995, *ApJS*, 101, 117
- Kenyon, S. J., Gomez, M., Whitney, B. 2008, to appear in the *Handbook of Star Forming Regions*, ASP Monograph Series
- Kessler-Silacci, J., Augereau, J., Dullemond, C. P. et al. 2006, *ApJ*, 639, 275
- Kessler-Silacci, J., E., Dullemond, C. P., Augereau, J.-C. et al. 2007, *ApJ*, 659, 680
- Kissel, J. & Krueger, F. R. 1987, *Nature* 326, 755
- Lahuis, F. & van Dishoeck, E. F. 2000, *A&A*, 355, 699
- Lahuis, F., van Dishoeck, E. F., Boogert, A. C. A. et al. 2006, *ApJ*, L636, 145
- Lahuis, F., van Dishoeck, E. F., Blake, G. A. et al. 2007, *ApJ*, 665, 492
- Lee, L. C. 1984, *ApJ*, 282, 172
- López Martí, B.; Eisloffel, J., Scholz, A., Mundt, R. 2004, *A&A*, 416, 555
- Luhman, K. L. 2004, *ApJ*, 602, 816

- Luhman, K. L., Lada, C. J., Hartmann, L. et al. 2005, *ApJ*, L631, 69
- Luhman, K. L. 2007, *ApJS*, 173, 104
- Luhman, K. L. et al. 2008, *ApJ*, 675, 1375
- Luhman, K. L. 2008, to appear in the Handbook of Star Forming Regions, ASP Monograph Series
- Magee-Sauer, K., Mumma, M. J., DiSanti, M. A., Dello Russo, N. 2002, *Journal of Geophysical Research*, 107, 6
- Mathis, J. S. 1990, *ARA&A*, 28, 37
- Matsuyama, I., Johnstone, D., Hartmann, L. 2003, *ApJ*, 582, 893
- Meyer, M. R. et al. 2004, *ApJS*, 154, 422
- Meyer, M. R. et al. 2006, *PASP*, 118, 1690
- Meyer, M. R., Backman, D. E., Weinberger, A. J., Wyatt, M. C. in *Protostars and Planets V*, 573
- Mohanty S., Jayawardhana, R., Natta, A., Fujiyoshi, T., Tamura, M., Barrado y Navascués, D. 2004, *ApJ*, L609, 33
- Muzerolle, J., Luhman, K. L., Briceno, C., Hartmann, L., Calvet, N. 2005, *ApJ*, 625, 906
- Najita, J. R., Strom, S. E., Muzerolle, J. 2007, *MNRAS*, 378, 369
- Natta A., Testi, L., Muzerolle, J., Randich, S., Comerón, F., Persi, P. 2004, *A&A*, 424, 603
- Oro, J. 1960, *Biochem. Biophys. Res. Comm.*, 2, 407
- Pascucci, I., Apai, D., Henning, Th., Dullemond, C. P. 2003, *ApJ*, L590, 111

- Pascucci, I., Gorti, U., Hollenbach, D. et al. 2006, *ApJ*, 651, 1177
- Pascucci, I., Hollenbach, D., Najita, J. et al. 2007, *ApJ*, 663, 383
- Pascucci, I., Apai, D., Hardegree-Ullman, E. E., Kim, J. S., Meyer, M. R., Bouwman, J.
2008, *ApJ*, 673, 477
- Pascucci, I. & Tachibana, S. 2009, to appear in the book *Protoplanetary Dust*, eds. D. Apai
& D. Lauretta (Cambridge University Press)
- Persi, P., Marenzi, A. R., Olofsson, G. et al. 2000, *A&A*, 357, 219
- Riaz & Gizis 2008, *ApJ*, 681, 1584
- Scholz, A., Jayawardhana, R., Wood, K., Meeus, G., Stelzer, B., Walker, C., O'Sullivan, M.
2007, *ApJ*, 660, 1517
- Shapiro, R. 1995, *Origins of Life and Evolution of the Biosphere* 25, Issue 13, 83
- Semenov, D., Wiebe, D., Henning, Th. 2004, *A&A*, 417, 93
- Sicilia-Aguilar, A., Hartmann, L. W., Furész, G., Henning, Th., Dullemond, C., Brandner,
W. 2006, *AJ*, 132, 2135
- Sicilia-Aguilar, A., Hartmann, L. W., Watson, D., Bohac, C., Henning, Th., Bouwman, J.
2007, *ApJ*, 659, 1637
- Sterzik, M. F., Pascucci, I., Apai, D., van der Blik, N., Dullemond, C. P. 2004, *A&A*, 427,
245
- Stoks, P. G. & Schwartz, A. W., 1981, *Geochimica et Cosmochimica Acta*, 45, 563
- van Boekel, R., Waters, L. B. F. M., Dominik, C., Bouwman, J., de Koter, A., Dullemond,
C. P., Paresce, F. 2003, *A&A*, 400L, 21

van Boekel, R., Min, M., Waters, L. B. F. M., de Koter, A., Dominik, C., van den Ancker, M. E., Bouwman, J. 2005, *A&A*, 437, 189

van Dishoeck, E. F., Jonkheid, B., van Hemert, M. C. eprint arXiv:0806.0088

White, R. J. & Basri, G. 2003, *ApJ*, 582, 1109

Wooden, D., Desch, S., Harker, D., Gail, H.-P., Keller, L. 2007, in *Protostars and Planets V*, 815

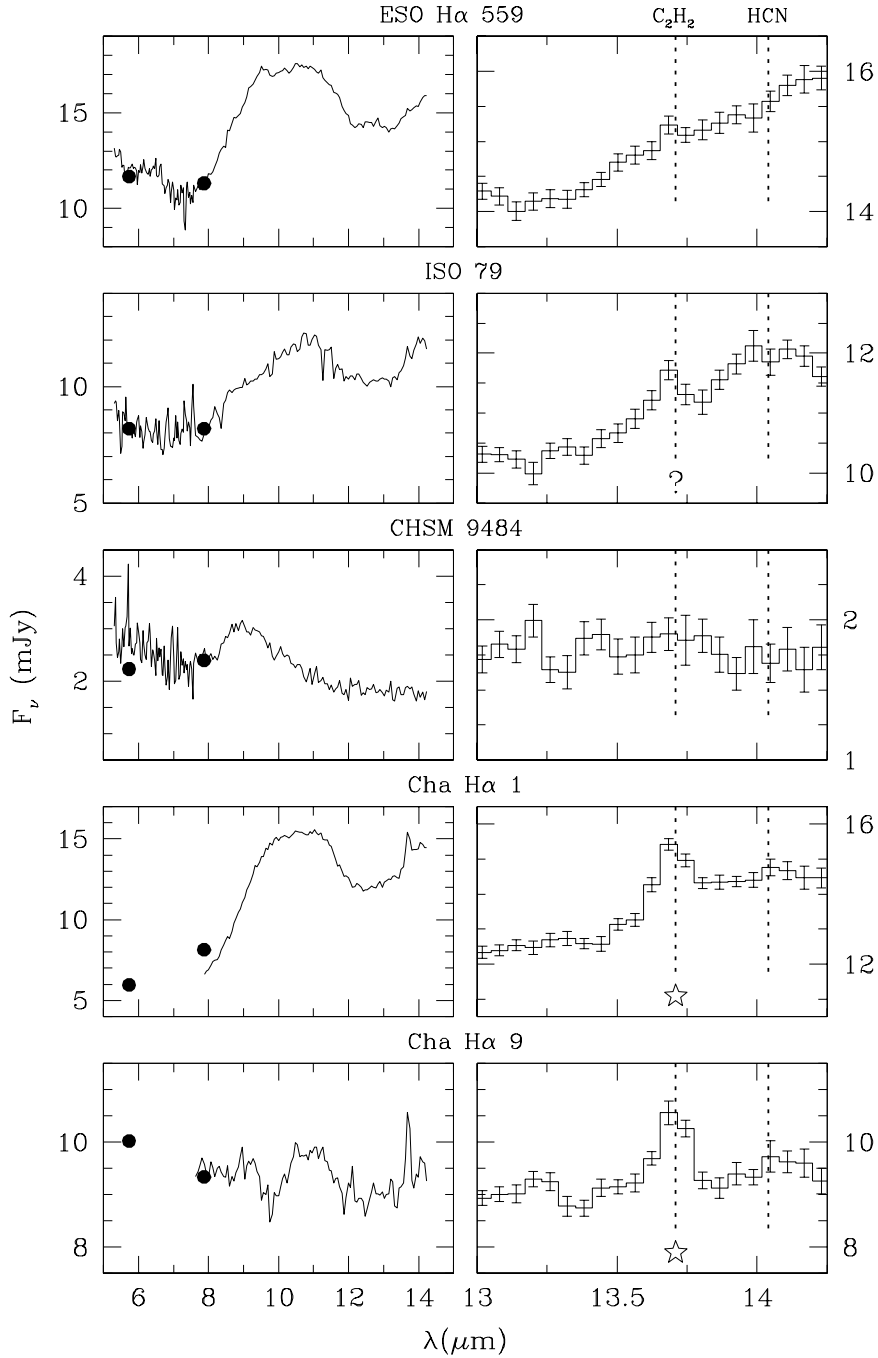


Fig. 1.— Left Panels: IRS low-resolution spectra for the cool star sample. The IRAC 5.8 and 8 μm fluxes from Luhman et al. (2008a) are over-plotted as filled black circles (when multiple observations are available we plot the mean flux values). Right Panels: Expanded view of the brown dwarf spectra around the C₂H₂ and HCN emission bands. A star indicates a “firm” detection while a question mark indicates a “possible” detection.

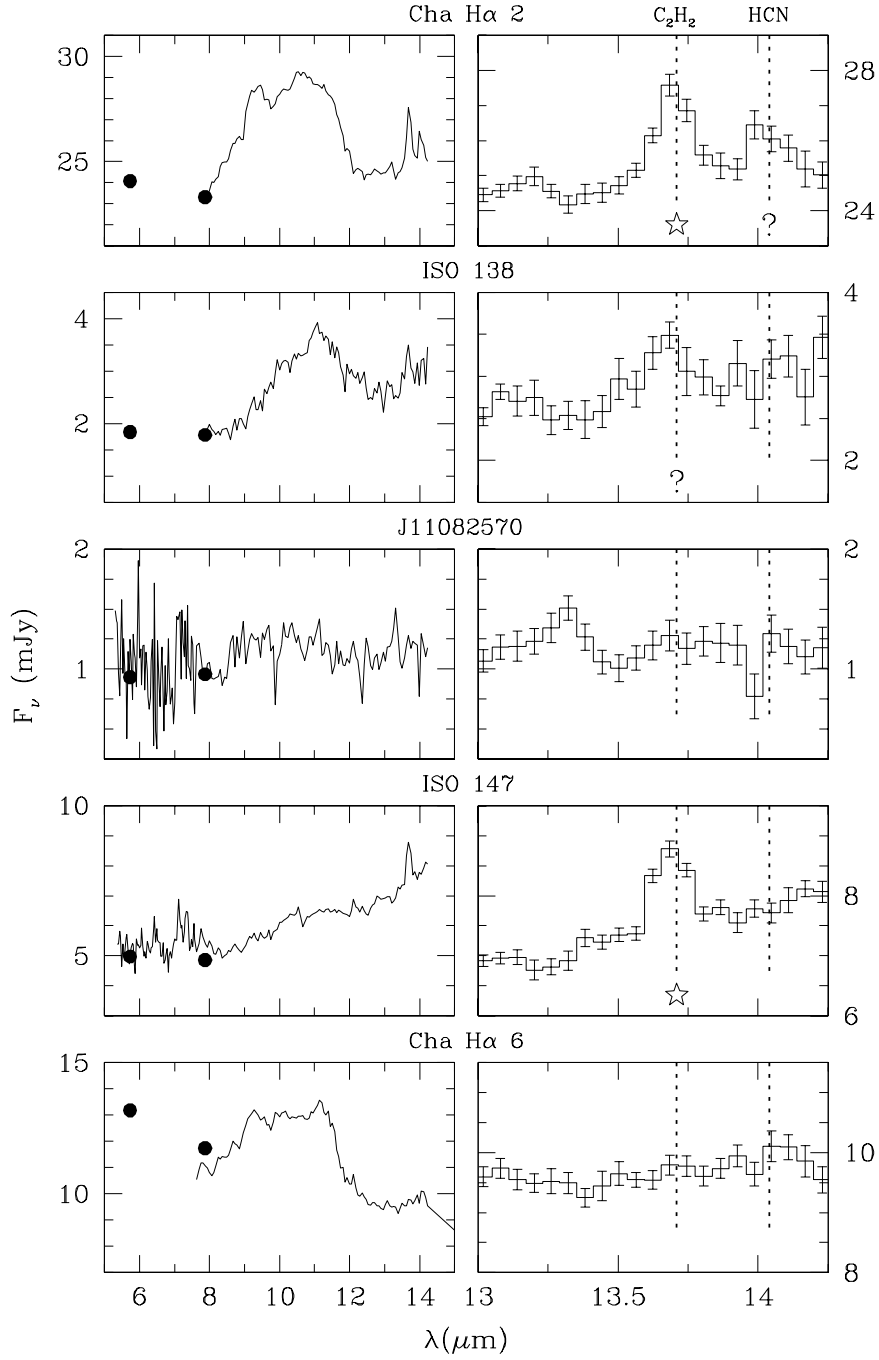


Fig. 2.— Same as Fig. 1.

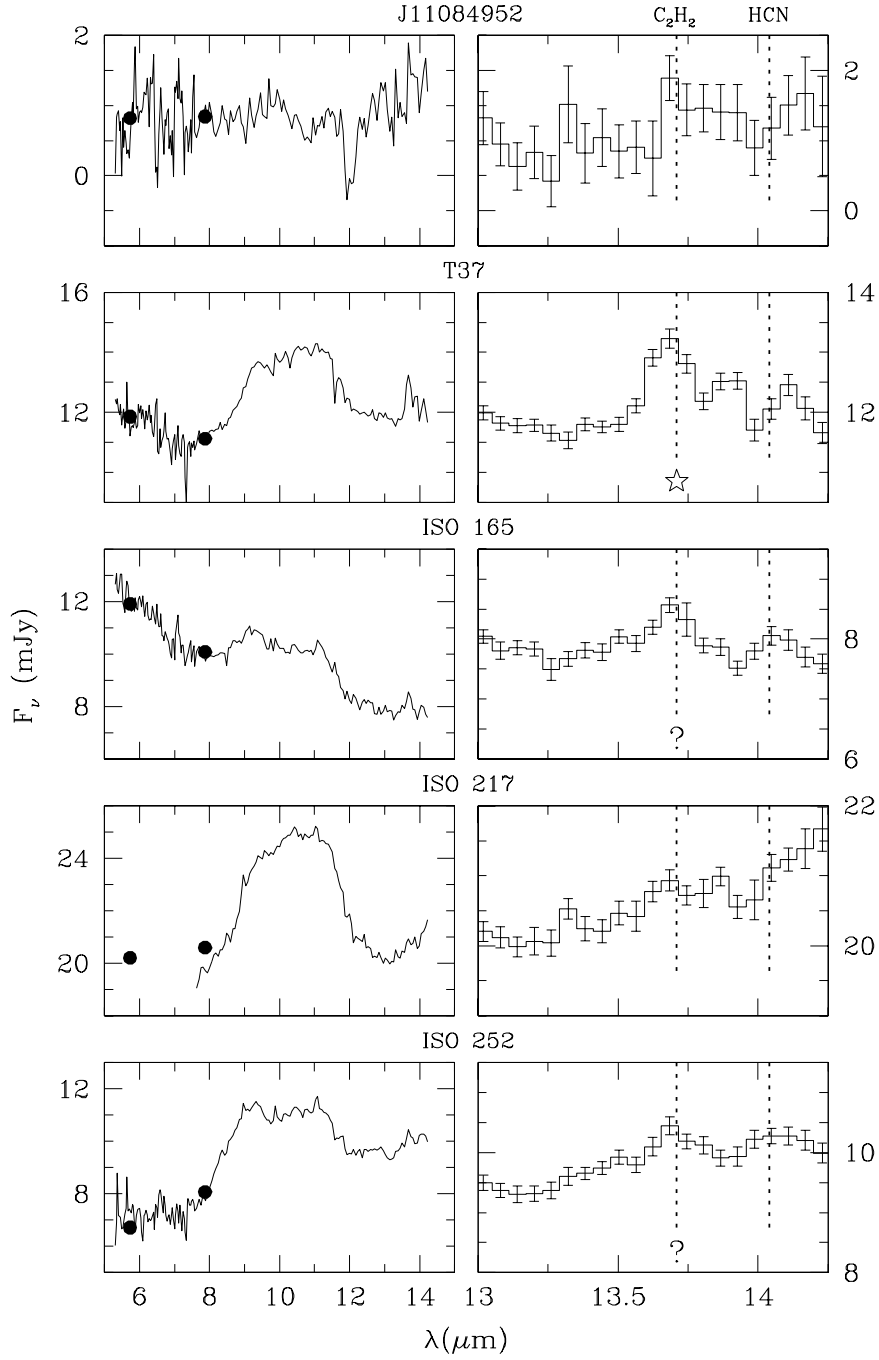


Fig. 3.— Same as Fig. 1.

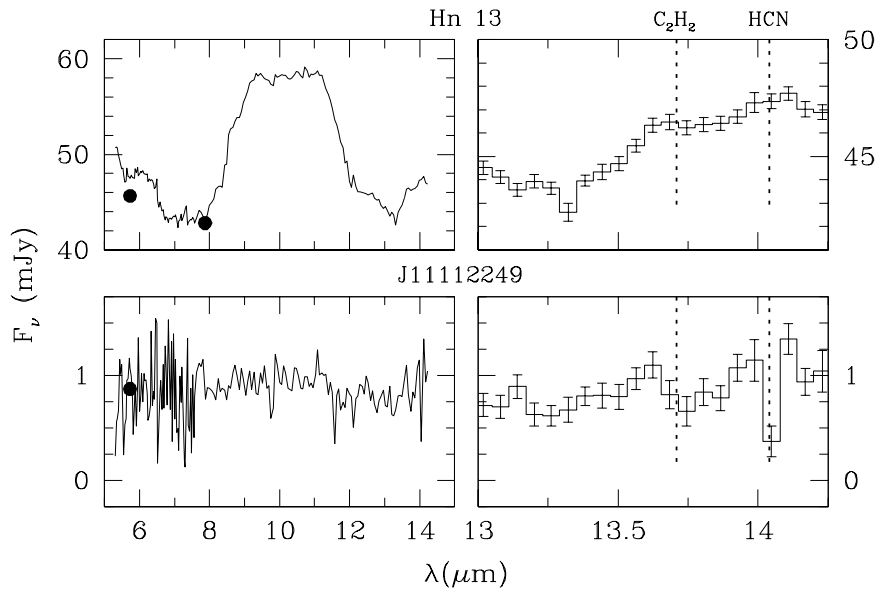


Fig. 4.— Same as Fig. 1.

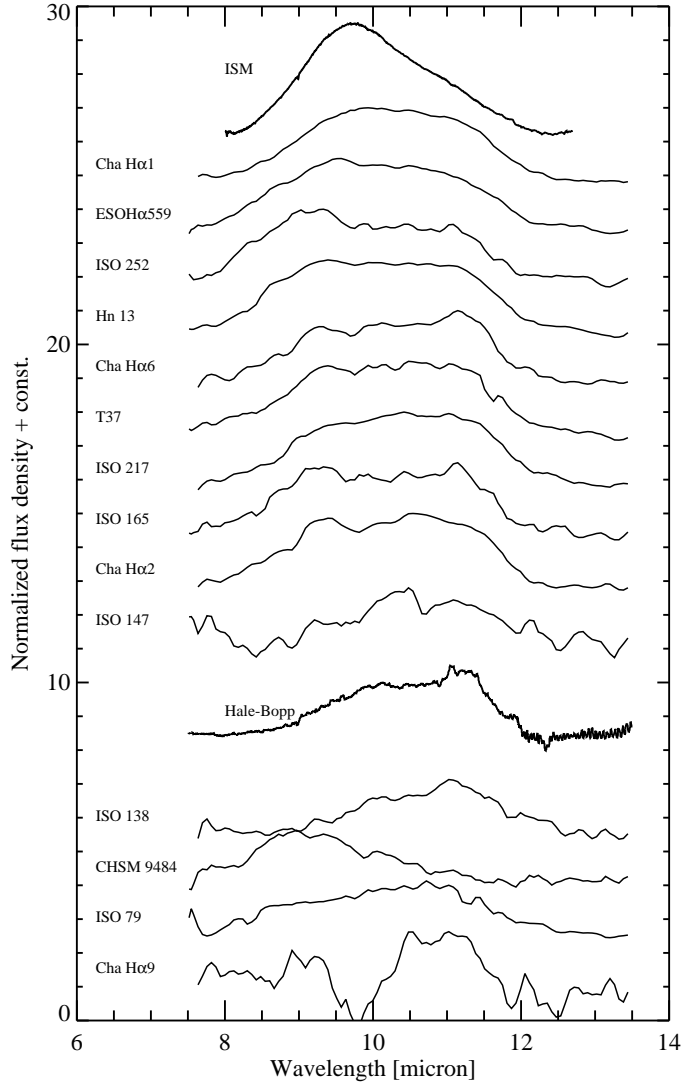


Fig. 5.— Qualitative comparison of the $10\ \mu\text{m}$ silicate emission features from cool star disks. Spectra have been continuum-subtracted and normalized to the peak emission. For comparison the spectra of the amorphous silicate-dominated ISM (Kemper et al. 2005) and the crystalline-rich comet Hale-Bopp (Crovisier et al. 1997) are also shown.

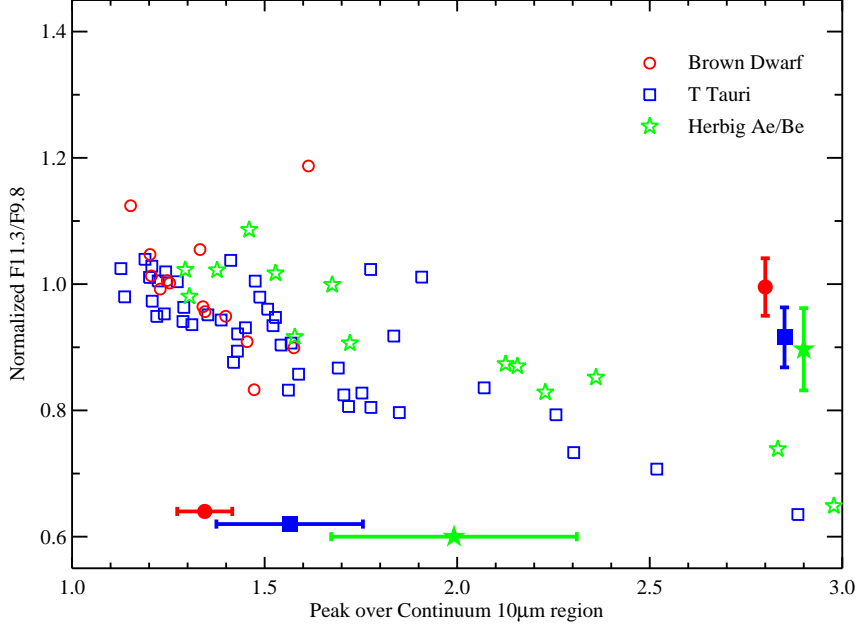


Fig. 6.— Shapes and strengths of the $10\ \mu\text{m}$ emission features for the samples of Herbig Ae/Be stars (green stars), sun-like/T Tauri stars (blue squares), and cool stars/brown dwarfs (red circles). On the y-axis we plot the ratios of the normalized flux at $11.3\ \mu\text{m}$ over $9.8\ \mu\text{m}$, which are proxies for the degree of crystallinity. The x-axis gives the peak over continuum in the $10\ \mu\text{m}$ region of normalized spectra, which indicates the amount of grain growth. The filled symbols with errorbars show the mean values and the 1σ standard deviations of the peak-over-continuum and of the F11.3/F9.8 for the three groups of disks. Cool star disks have statistically weaker $10\ \mu\text{m}$ features than Herbig Ae/Be disks.

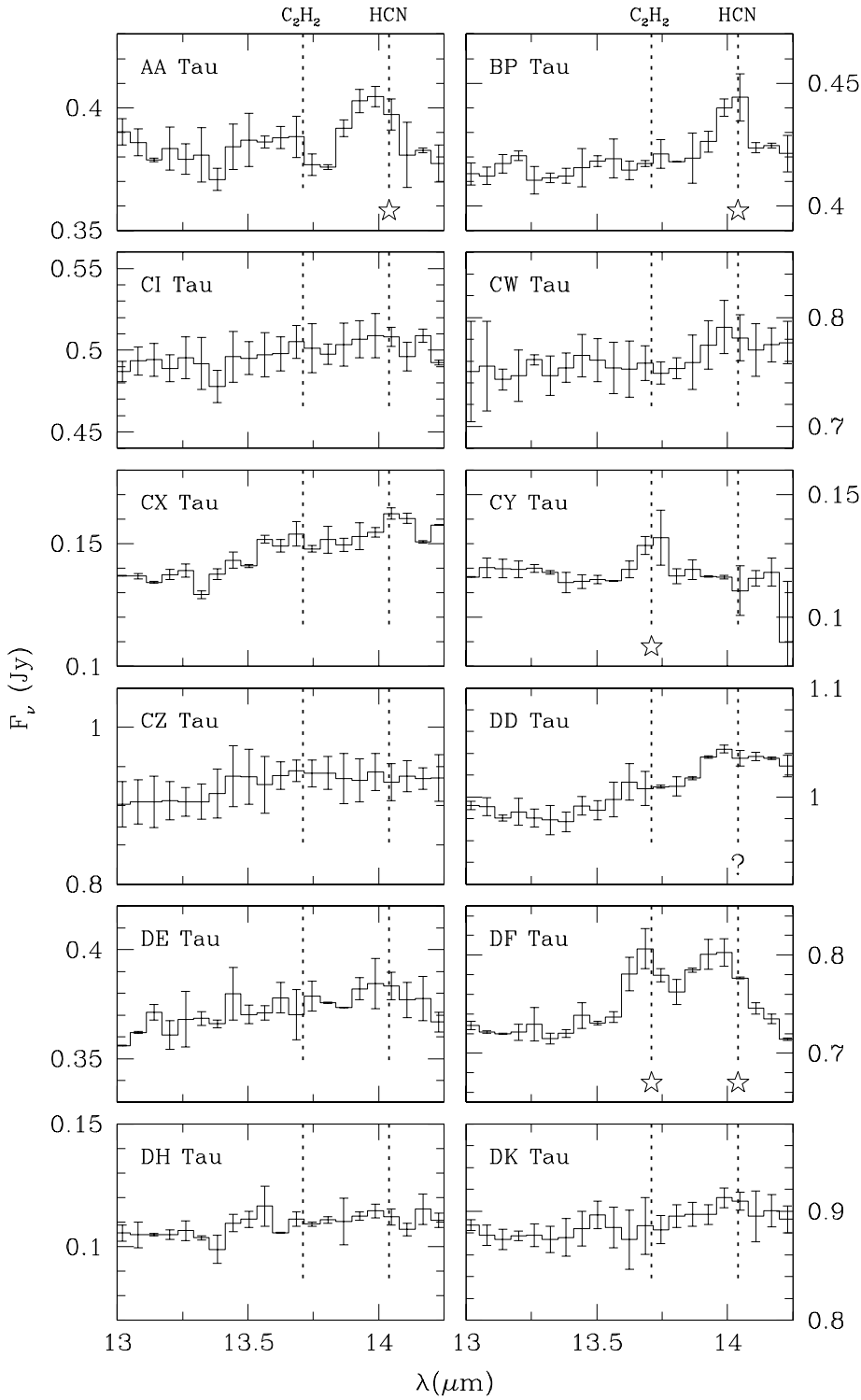


Fig. 7.— Expanded view of the sun-like spectra around the C₂H₂ and HCN emission bands. A star indicates a “firm” detection while a question mark indicates a “possible” detection. The full spectra are presented in Pascucci et al. (2008).

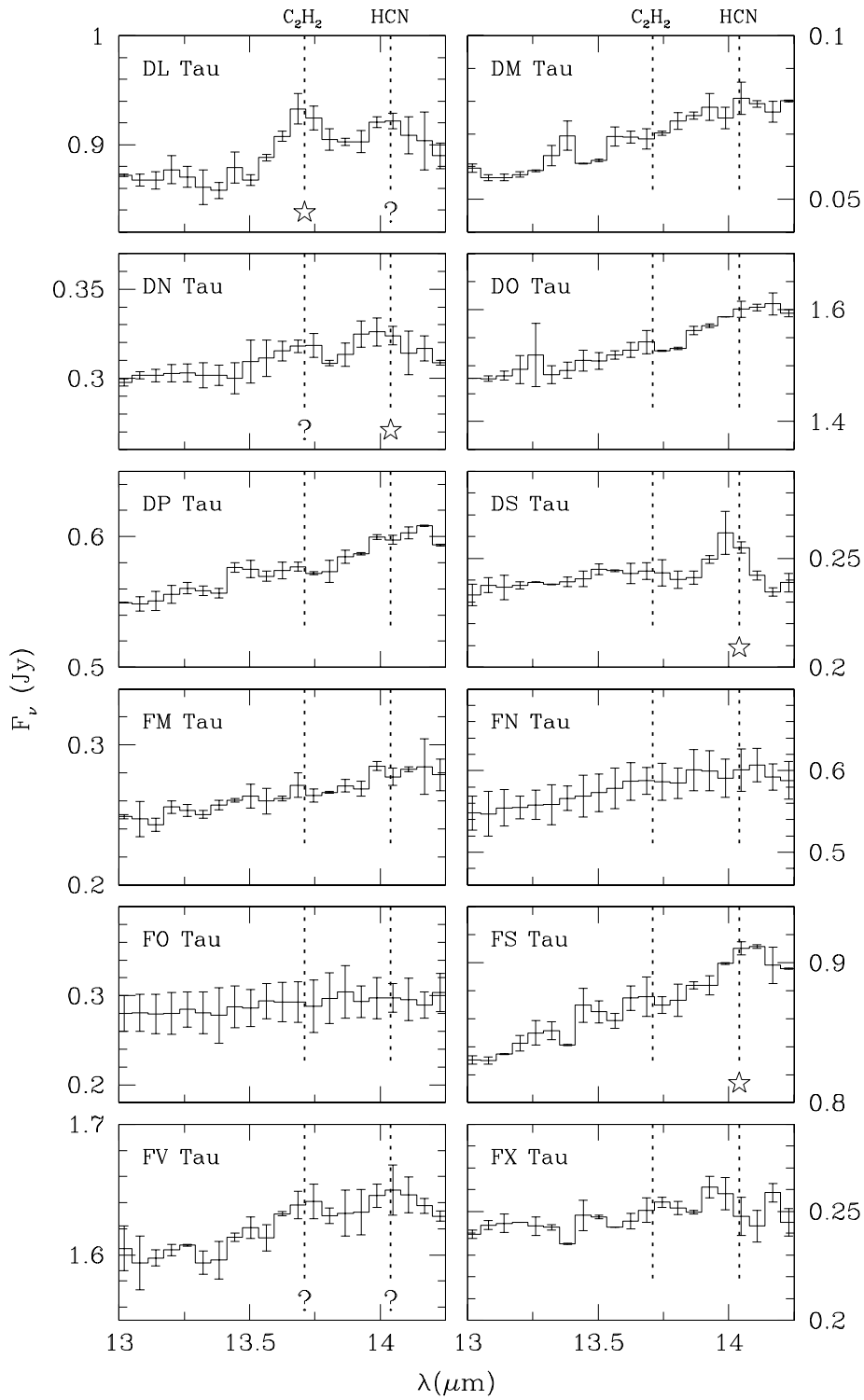


Fig. 8.— Same as Fig. 7.

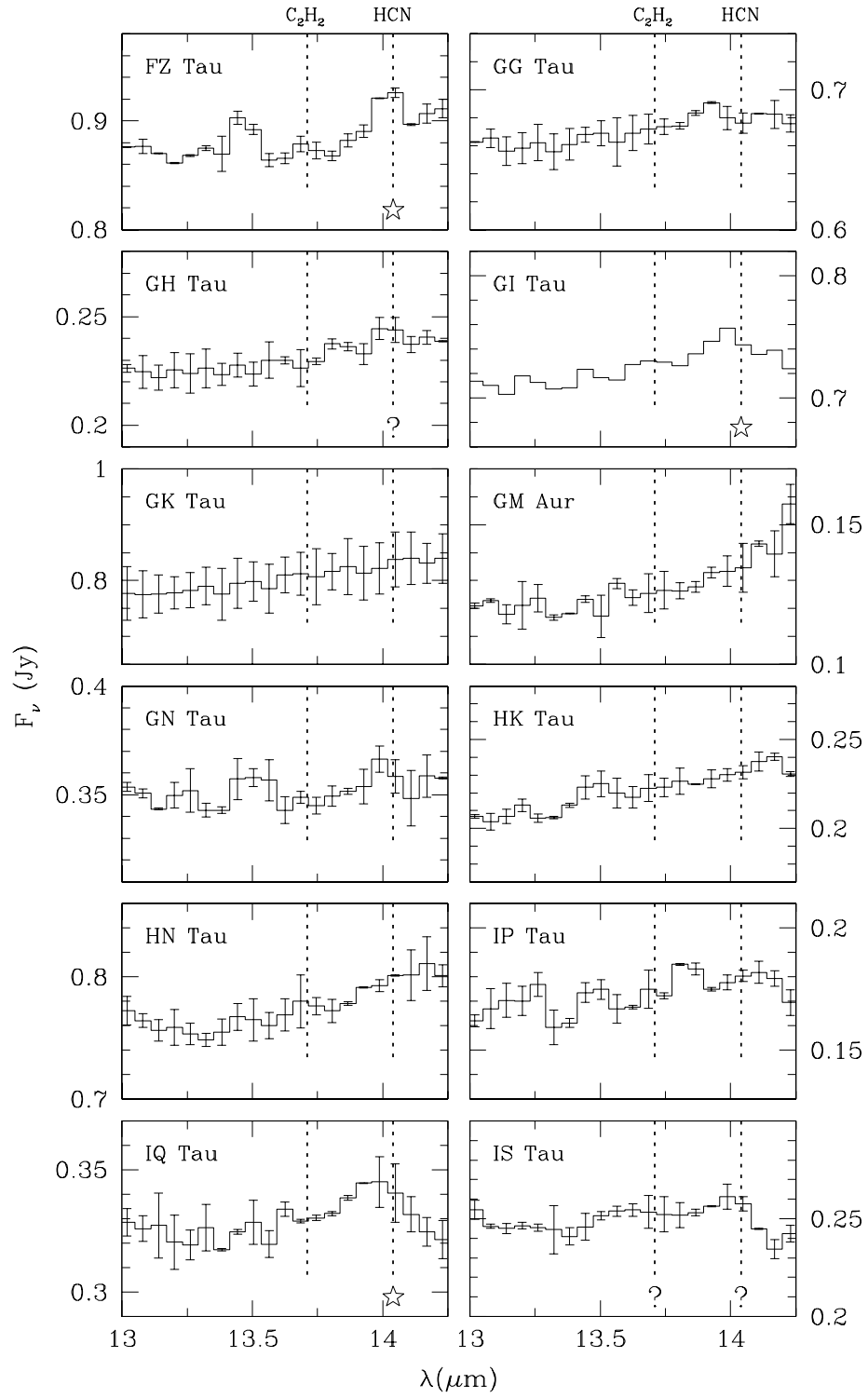


Fig. 9.— Same as Fig. 7.

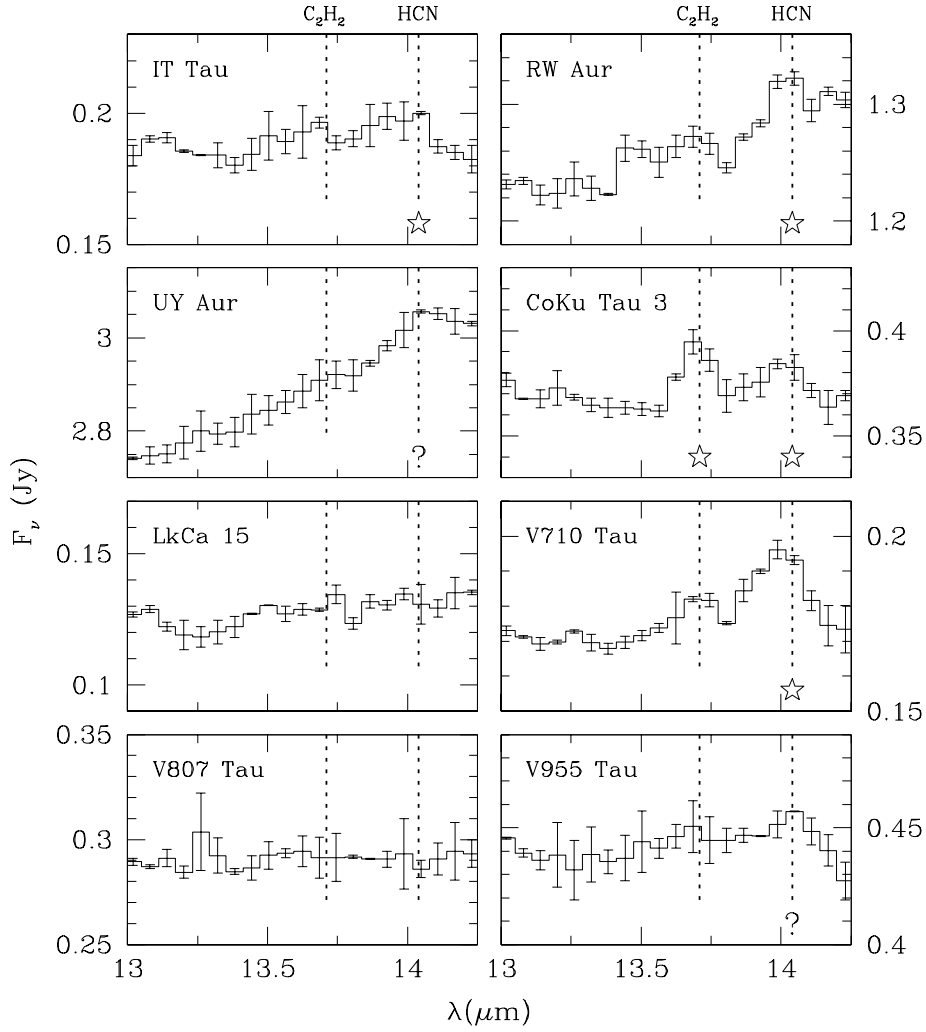


Fig. 10.— Same as Fig. 7.

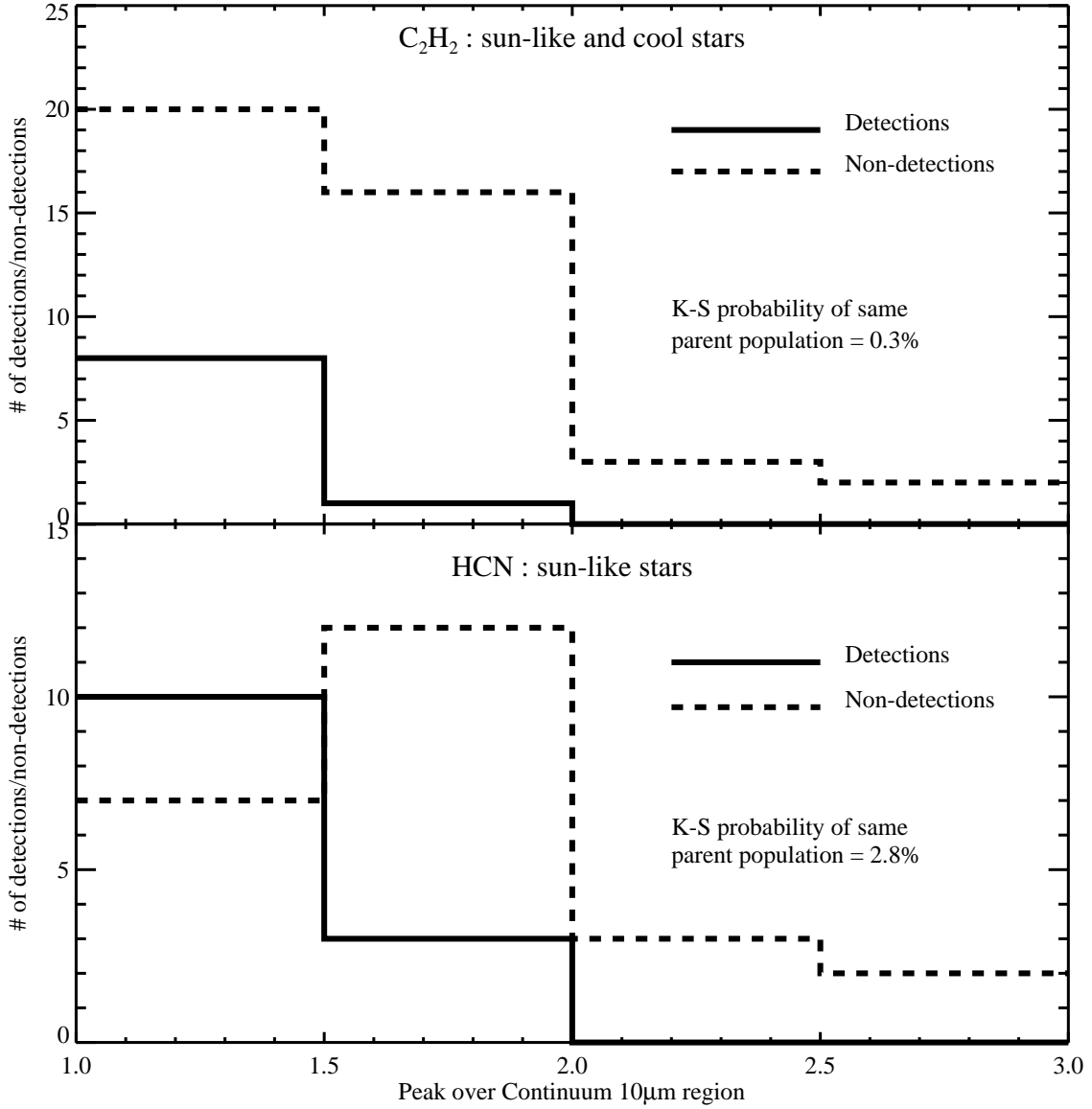


Fig. 11.— Upper Panel: Histogram of the $10\mu\text{m}$ silicate feature strengths for the detections (solid line) and non-detections (dashed line) of the C_2H_2 emission band in the combined sample of disks around sun-like and cool stars. Lower Panel: Histogram of the $10\mu\text{m}$ feature strengths for the detections (solid line) and non-detections (dashed line) of the HCN emission band in the sample of disks around sun-like stars (no cool star spectrum presents a firm HCN detection). Both panels show that detections are confined to weak features (peak-over-continuum ratios < 2). The K-S probabilities that C_2H_2 and HCN detections and non-detections are drawn from the same parent population are only 0.3 and 2.8% respectively.

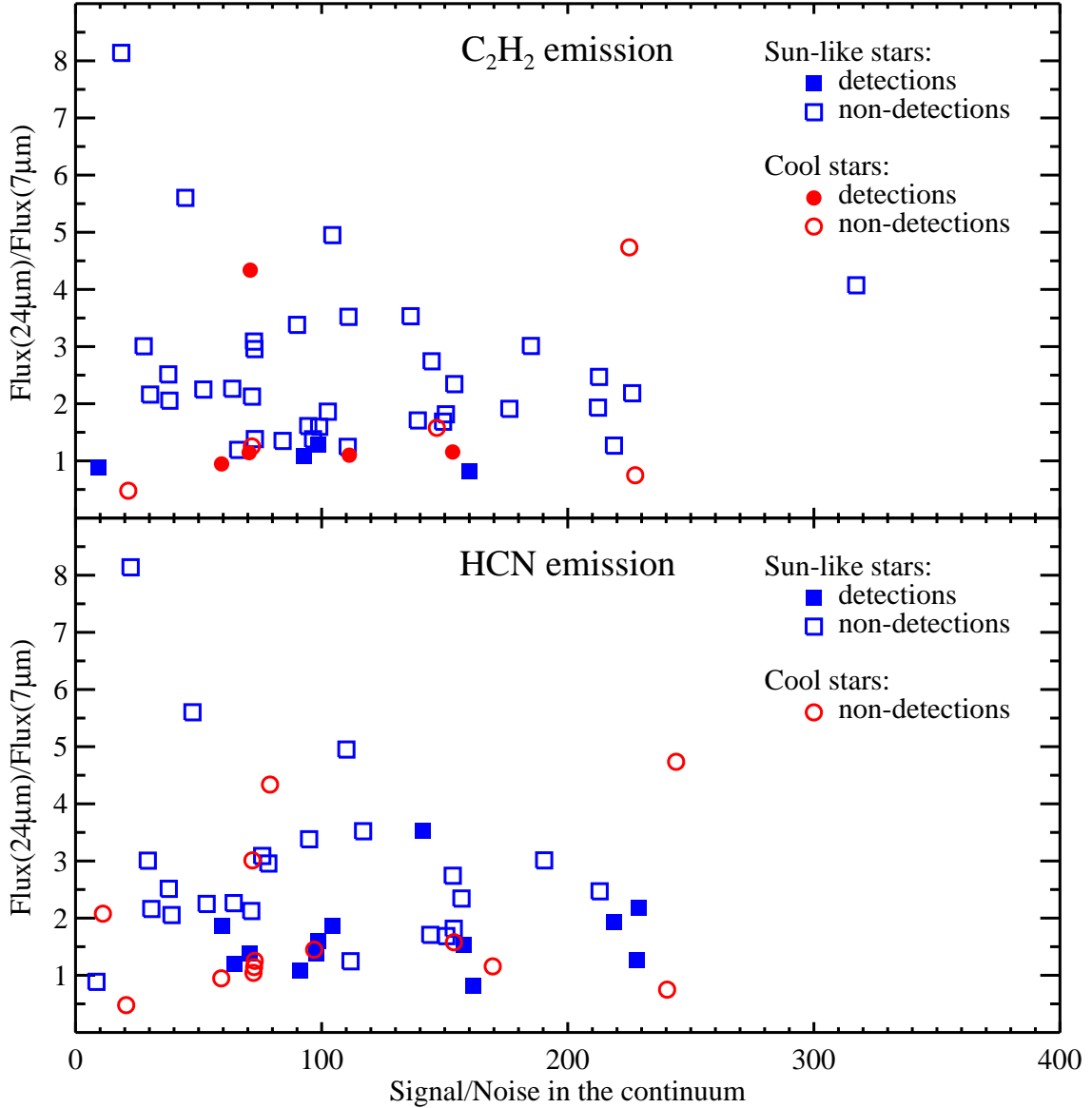


Fig. 12.— Upper Panel : Flux ratios at 24 over $7\mu\text{m}$ versus the signal-to-noise in the continuum close to the rovibrational emission bands of C_2H_2 and HCN. Fluxes at $24\mu\text{m}$ are from Pascucci et al. (2008) and Luhman et al. (2008a). Flatter disk structures are indicated by lower flux ratios in the figure. Detections of the C_2H_2 band are filled symbols, non-detections are empty symbols (“possible” detections are omitted). Squares are for sun-like stars, circles for cool stars. Lower Panel : Same as upper panel but for the HCN emission band. No cool star spectrum presents a “firm” HCN detection. C_2H_2 as well as HCN detections are confined to low flux ratios, indicative of flatter disk structures. The figure demonstrates that the pattern of the gas line detections are not primarily set by the signal-

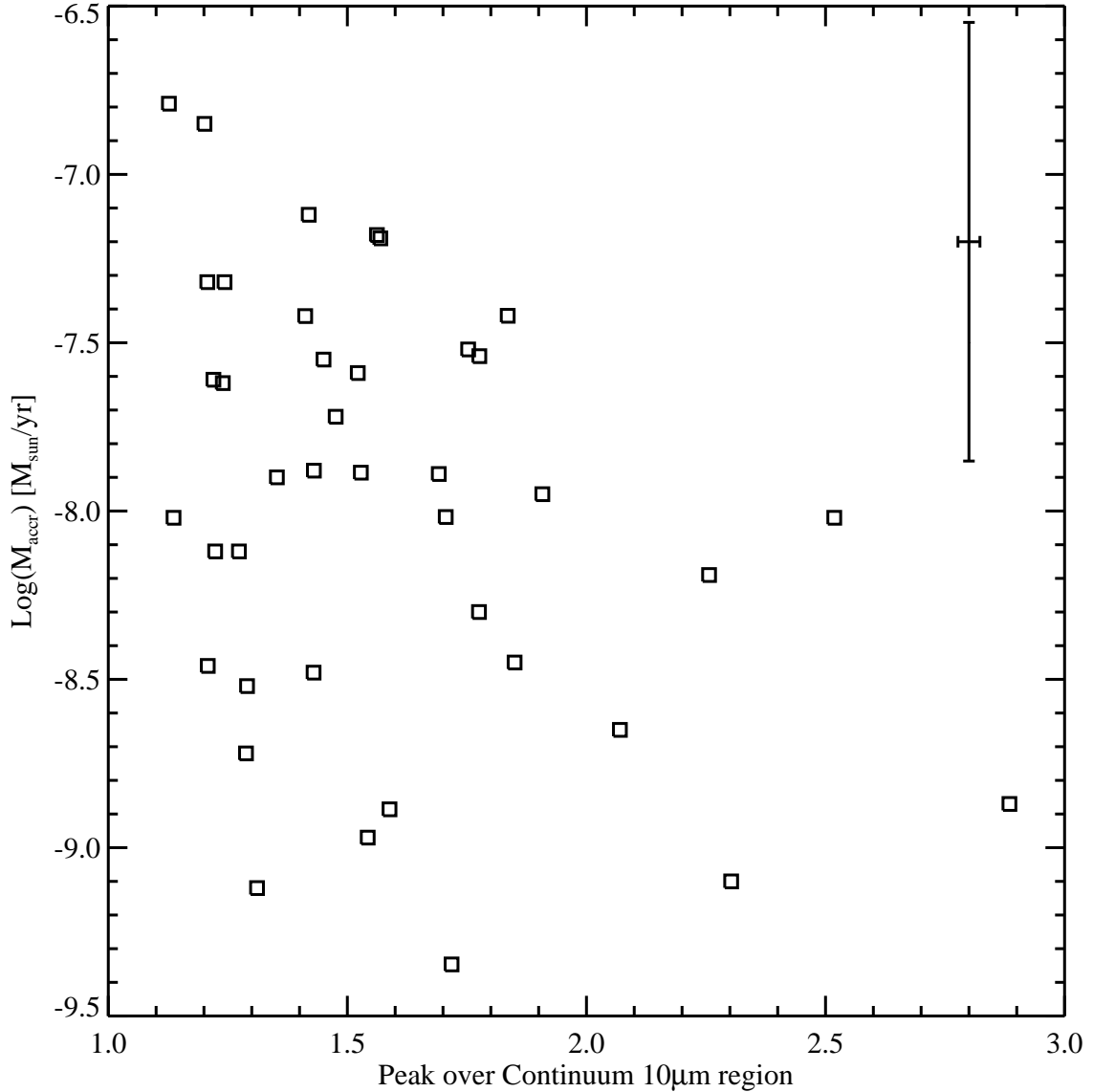


Fig. 13.— Stellar accretion rate (M_{accr}) versus $10\mu\text{m}$ feature strength for the sample of sun-like stars. Accretion rates are from the literature (Hartigan et al. 1995; Hartmann et al. 1998; Gullbring et al. 1998; White & Basri 2003; Najita et al. 2007) and have been placed on a consistent scale using the factors calculated in Najita et al. (2007). FM Tau, CoKu Tau 3, IT Tau, and V710 Tau do not have measured accretion rates. The errorbar on the peak-over-continuum is from Pascucci et al. (2008) while the uncertainty in the mass accretion rate is from Najita et al. (2007). There is a 4% probability that the data are randomly distributed, the negative Kendall rank correlation coefficient (-0.22) indicates a moderate anti-correlation. Yet, given the large uncertainty in the mass accretion rate we are cautious

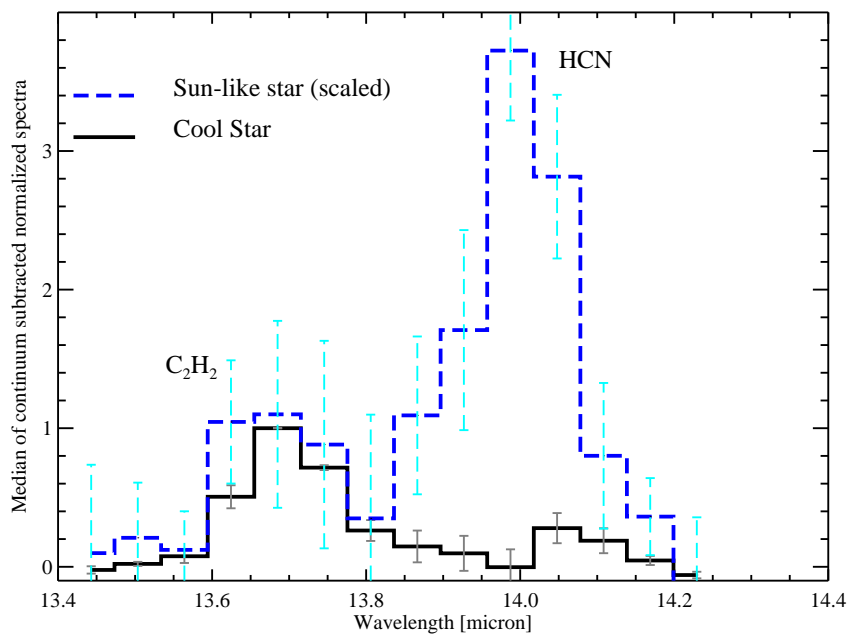


Fig. 14.— Median of continuum-subtracted and normalized spectra for the sun-like star (blue) and the cool star (black) samples presenting C₂H₂ and/or HCN emission bands (5 cool stars and 15 sun-like stars). The spectra are normalized to the peak of emission and scaled to match the C₂H₂ emission in the two samples. The errorbars are the standard deviations of the normalized spectra. If cool stars had the same flux ratio of HCN versus C₂H₂ as the sun-like stars do, HCN emission would have been easily detected toward them.

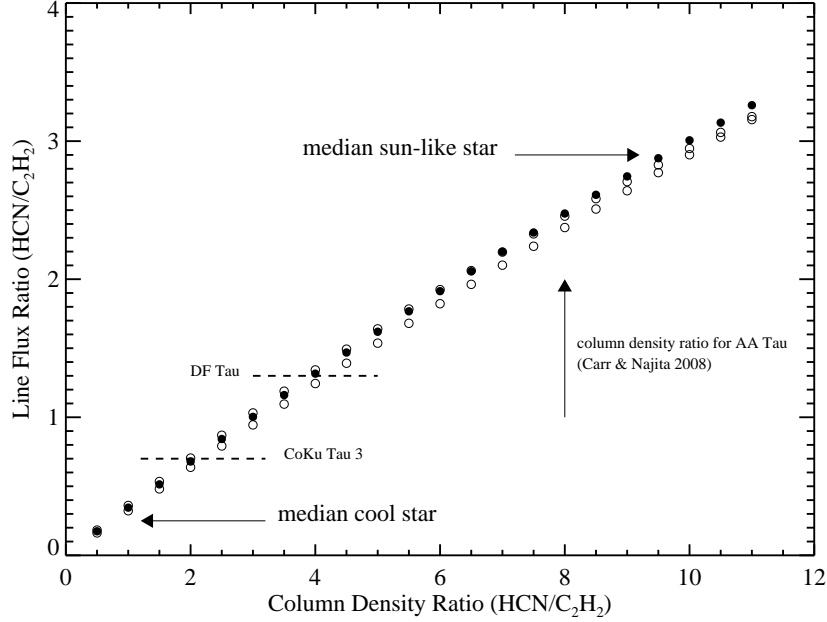


Fig. 15.— Line flux ratio of HCN over C_2H_2 versus column density ratio of the two molecules. Circles are values predicted from synthetic spectra calculated following Lahuis & van Dishoeck (2000). The C_2H_2 column density is kept fixed at 10^{16} cm^{-2} while the HCN column density varies from $0.5\text{-}11 \times 10^{16} \text{ cm}^{-2}$, thus covering the C_2H_2 and HCN column densities reported by Carr & Najita (2008) for AA Tau. Filled circles are for a gas temperature of 650 K while empty circles are for gas at 450 and 850 K. Arrows indicate the line flux ratios measured from the median cool star and sun-like star spectra in Fig. 14. The dashed lines report the HCN over C_2H_2 flux ratios for the only two sources in our sample where both molecular lines are firmly detected. The figure illustrates that the large difference in the HCN/ C_2H_2 flux ratio between the cool star and the sun-like star samples translates into very different column density ratios of the two molecules. We note that in the case of AA Tau Carr & Najita (2008) find an HCN/ C_2H_2 column density ratio of 8, similar to what we require for the median spectrum of the sun-like stars.

Table 1. Sample of cool stars in the Cha I star-forming region identified via infrared photometry.

Source	2MASS J ^a	Sp. Type	$F_{6.7\mu m}$ (mJy)	$F_{14.3\mu m}$ (mJy)	$F_{8\mu m}$ (mJy)	Other name
Hn 2*	11034764-7719563	M5	11.4±0.8	3.7±1.0	9.1	ChaI 425,ISO 32
CHXR 15*	11054300-7726517	M5.25	13.2±1.1	–	8.5	ChaI 449,ISO 65
ESO-H α 559	11062554-7633418	M5.25	–	–	11.4	
ISO 79	11063945-7736052	M5.25	8.0±2.0	9.9±1.5	8.2	
CHSM 9484	11071181-7625501	M5.25	–	–	2.4	ChaI 711
Cha H α 1	11071668-7735532	M7.75	6.7±1.8	11.8±1.5	8.1	ISO 95
Cha H α 9	11071860-7732516	M5.5	11.4±0.9	9.2±1.3	9.4	ISO 98
Cha H α 2	11074245-7733593	M5.25	24.5±1.4	23.4±1.2	23.3	ISO 111
ISO 138	11081850-7730408	M6.5	15.3±0.8	17.6±1.3	1.8	ChaI 410
J11082570-7716396	11082570-7716396	M8	–	–	1.0	
ISO 147	11082650-7715550	M5.75	4.3±1.1	–	4.7	
Cha H α 6	11083952-7734166	M5.75	12.7±1.5	–	11.8	ISO 152
J11084952-7638443	11084952-7638443	M8.75	–	–	0.8	
T37	11085090-7625135	M5.25	7.5±1.5	–	11.1	ISO 157
ISO 165	11085497-7632410	M5.5	12±1.8	–	10.1	
ISO 217	11095215-7639128	M6.25	10.3±2.5	–	20.7	ChaI 726
ISO 252	11104141-7720480	M6	5.5±0.8	6.8±1.2	8.1	
Hn 13	11105597-7645325	M5.75	31.4±1.8	27.5±1.9	44.4	ISO 259
J11112249-7745427 ^b	11112249-7745427	M8.25	–	–	–	

Note. — All spectral types are from Luhman (2004); Luhman et al. (2008a) and Luhman et al. (2005). They are determined from optical spectra and have typical precisions of 0.25. Fluxes at 6.7 and 14.3 μm are from Persi et al. (2000), while fluxes at 8 μm are from Luhman et al. (2008a). The 8 μm IRAC fluxes are mean values of fluxes from multiple campaigns.

^aThe 2MASS source name includes the J2000 sexagesimal, equatorial position in the form: hhmmssss+ddmmss (Cutri et al. 2003).

*The IRS spectra are consistent with photospheric emission, see text.

^bThis source has no 8 μm IRAC data but has excess emission at 5.8 μm

Table 2. Log of the observations.

Source	Date	Peak-up	Exposure Times		
	mm/dd/year	Mode	SL1	SL2	LL1
Hn 2	03/12/2005	PCRS	60s×20	–	30s×36
CHXR 15	03/12/2005	PCRS	60s×20	–	30s×36
ESO-H α 559	08/02/2006	PCRS	60s×40	60s×12	–
ISO 79	03/13/2007	PCRS	60s×40	60s×10	–
CHSM 9484	08/02/2006	PCRS	60s×40	60s×12	–
Cha H α 1	03/12/2005	PCRS	60s×20	–	–
Cha H α 9	03/12/2005	PCRS	60s×20	–	30s×36
Cha H α 2	03/12/2005	PCRS	60s×14	–	–
ISO 138	03/12/2005	PCRS	60s×14	–	–
J11082570-7716396	03/11/2007	PCRS	60s×40	60s×12	–
ISO 147	03/11/2007	PCRS	60s×40	60s×12	–
Cha H α 6	03/12/2005	PCRS	60s×20	–	30s×36
J11084952-7638443	03/11/2007	IRS	60s×40	60s×12	–
T37	07/25/2006	PCRS	60s×40	60s×10	–
ISO 165	08/02/2006	PCRS	60s×40	60s×12	–
ISO 217	03/12/2005	IRS	60s×20	–	30s×36
ISO 252	03/11/2007	PCRS	60s×40	60s×12	–
Hn 13	03/11/2007	IRS	60s×40	60s×12	–
J11112249-7745427	08/02/2006	PCRS	60s×40	60s×10	–

Table 3. Statistics on the firm detections of HCN and C₂H₂ from the sun-like and cool stars with disks. Because the sun-like stars were selected to have silicate emission features, we have excluded from the cool star sample the 3 featureless cool stars (J11082570, J11084952, and J11112249). Also shown in the Table are the mean stellar temperatures, masses, radii, and accretion rates, used to compute the accretion luminosities. Values for individual stars are from Apai et al. (2005); Luhman (2007); Pascucci et al. (2008); Kenyon & Hartmann (1995); Najita et al. (2007); White & Basri (2003); Natta et al. (2004); Muzerolle et al. (2005).

Sample	C ₂ H ₂ detections	HCN detections	$\langle T_\star \rangle$ [K]	$\langle M_\star \rangle$ [M _⊙]	$\langle R_\star \rangle$ [R _⊙]	$\langle \dot{M} \rangle$ M _⊙ /yr
Sun-like stars	4/44	13/44	3,900	0.8	2.1	1.3×10^{-8}
Cool stars	5/14	0/14	3,000	0.1	0.7	$< 3 \times 10^{-11}$